Quantitative analysis for detection and grading of hepatocellular carcinoma: Comparison of diffusion kurtosis imaging, intravoxel incoherent motion and conventional diffusion-weighted imaging

HONG-WEI LI[1,2*], GAO-WU YAN[3*], JIN YANG[4*], LI-HUA ZHUO[1], ANUP BHETUWAL[2], YONG-JUN LONG[1], XU FENG[2], HONG-CHAO YAO[1], XING-XIONG ZOU[1], RUO-HAN FENG[1], HAN-FENG YANG[2] and YONG DU[2]

[1]Department of Radiology, The Third Hospital of Mianyang, Sichuan Mental Health Center, Mianyang, Sichuan 621000; [2]Sichuan Key Laboratory of Medical Imaging and Department of Radiology, Affiliated Hospital of North Sichuan Medical College, Nanchong, Sichuan 637000; [3]Department of Radiology, Suining Central Hospital, Suining, Sichuan 629000; [4]Department of Nursing, The Third Hospital of Mianyang, Sichuan Mental Health Center, Mianyang, Sichuan 621000, P.R. China

Received March 2, 2022; Accepted August 10, 2022

DOI: 10.3892/ol.2022.13523

Abstract. The aim of the present study was to compare the diagnostic performance of the main parameters derived from diffusion kurtosis imaging (DKI), intravoxel incoherent motion (IVIM) and diffusion-weighted imaging (DWI) regarding the detection and grading of hepatocellular carcinoma (HCC). A total of 78 patients diagnosed with HCC by biopsy were prospectively enrolled in the present study, and underwent routine magnetic resonance imaging (MRI), DWI, IVIM, DKI and contrast-enhanced MRI prior to surgery. Measurements, including mean diffusivity (MD), mean diffusional kurtosis (MK), true diffusion coefficient (D), pseudo-diffusion coefficient (D^*), perfusion fraction (f) and apparent diffusion coefficient (ADC), were compared with grading HCC using one-way ANOVA followed by the Student-Neuman-Keuls-q post-hoc test. Spearman's correlation coefficient was used to analyze the correlation between each parameter and pathological grade, while the diagnostic efficiency was evaluated using a receiver operating characteristic (ROC) curve. The 78 patients enrolled in the present study were grouped into highly (n=22), moderately (n=41) or poorly (n=15) differentiated HCC groups according to the criteria of Pathology and Genetics Tumors of the Digestive System. MK values differed significantly between different grades and decreased gradually with the degree of tumor differentiation. The MD, D and ADC values in the highly differentiated HCC group were significantly higher than those in the moderately or poorly differentiated HCC groups (all P<0.001), whereas no significant differences were observed in D^* or f (P=0.502 and P=0.853, respectively). A significant correlation was observed between MK, MD, D and ADC, and HCC grades (r=0.705, r=0.570, r=0.423 and r=0.687, respectively). The comparison of the ROC curves of MK, MD, D, ADC, D^* and f values for predicting highly differentiated HCC suggested that MK and D were the best indicators for predicting highly differentiated HCC, as the area under the ROC curve (AUC) of MK and D was significantly higher than that of ADC (Z=2.247 and 2.428, P=0.025 and 0.016, respectively), whereas non-statistically significant differences were observed in the AUC values between MK and D (Z=0.072; P=0.942). The DKI-derived MK and IVIM-derived D values had a similar diagnostic performance and were superior to ADC in discriminating the histological grade of HCC. In addition, the combination of MK and D values exhibited an improved diagnostic performance.

Correspondence to: Dr Yong Du, Sichuan Key Laboratory of Medical Imaging and Department of Radiology, Affiliated Hospital of North Sichuan Medical College, 63 Wenhua Road, Nanchong, Sichuan 637000, P.R. China
E-mail: duyong@nsmc.edu.cn

*Contributed equally

Key words: hepatocellular carcinoma, histological grading, diffusion kurtosis imaging, diffusion-weighted imaging, intravoxel incoherent motion

Introduction

Hepatocellular carcinoma (HCC) is a common solid tumor, accounting for 841,000 new cases and 782,000 deaths each year, making it the sixth most common cancer type and the fourth leading cause of cancer death worldwide (1-3). Despite the recent advancements in surgical techniques, HCC still exhibits a high recurrence rate after tumor resection, which may hinder its treatment and the long-term survival of patients (4). Histological grade is a well-known prognostic factor for metastasis and recurrence following hepatic resection and transplantation. Previous studies have shown that poorly differentiated HCC is associated with worse overall survival and more frequent metastases and recurrence compared with highly and moderately differentiated HCC (5,6). Therefore, an

accurate preoperative diagnosis based on tumor pathological grade is of great importance for determining therapeutic strategies and assessing prognosis.

Magnetic resonance imaging (MRI), a constantly evolving technique, allows for uniform sampling of the whole tumor in HCC pathological grading. For instance, diffusion-weighted imaging (DWI), a non-invasive procedure with the absence of ionizing radiation, is effective in evaluating the microscopic mobility of water molecules within the tissue. However, microstructural barriers (such as cell membranes, organelles and microcirculation of blood in capillaries) restrict water diffusion, which changes the distribution into a non-Gaussian one. The standard DWI-derived apparent diffusion coefficient (ADC) value cannot accurately measure the real diffusivity, as it assumes a Gaussian distribution of displacements of diffusing spins corresponding to water molecules freely moving in the containing medium (7,8). Hence, MRI techniques with extended diffusion models, such as biexponential DWI and diffusion kurtosis imaging (DKI), may be able to offer precise information about water diffusion (9,10). Intravoxel incoherent motion (IVIM) with biexponential mode was first proposed by Le Bihan *et al* (11) in 1986 to quantitatively assess the microscopic translational motions that occur in each image voxel on MRI. In addition, using a biexponential model may distinguish the diffusion of water molecules from the micro-capillary perfusion of tissues and obtain diffusion parameters, including the true diffusion (D), pseudo-diffusion (D^*) and perfusion fraction (f). An alternative method, DKI, initially described by Jensen and Helpern (12) and Jensen *et al* (13), recommended the characterization of the non-Gaussian nature of water diffusion. The method, derived mathematically through the use of a polynomial model with a dimensionless factor called K, could provide additional microstructural information about tissue heterogeneity and cellularity with high b-values, and was successfully applied in subsequent diffusion studies (14,15). While preliminary studies have assessed the correlation between DWI and histological grade in HCC (16-19), Nasu *et al* (20) report inconclusive or conflicting results. Considering that mono and biexponential DWI and DKI are able to illustrate different tissue properties, this can be used to explore and compare their roles in the differentiation of histopathological grading in HCC. However, to the best of our knowledge, a limited number of studies have evaluated the associations between quantitative parameters derived from standard DWI, DKI and IVIM and histopathological grading in HCC. Therefore, the purpose of the present prospective study was to quantitatively correlate the ability of various diffusion parameters derived from DWI, IVIM and DKI for detecting and grading HCC.

Materials and methods

Patient population. The present study was approved by the Institutional Review Board of the Affiliated Hospital of North Sichuan Medical College (Nanchong, China; approval no. nsmc17-10). Written informed consent was obtained from each participant before the study. All methods were performed in accordance with the Declaration of Helsinki. Between January 2017 and March 2020, a total of 96 patients who received routine and contrast MRI, DWI, IVIM and DKI at the North Sichuan Medical College (Nanchong, China) for the detection of clinically suspected HCC, which was later confirmed and graded following histopathological examination either after post-surgical resection or through stereotactic biopsy specimen evaluation, were enrolled in the present study. Between pathological examination and MRI, the mean standard deviation was 4 days (range, 1-8 days). Upon review, 18 patients were excluded from the study for the following reasons: i) HCC tumor diameter <0.5 cm (n=3); ii) poor image quality or motion artifact (n=6); and iii) radiotherapy, chemotherapy, ablation or trans-catheter arterial chemoembolization received prior to MRI examination (n=9). Finally, 78 patients (25 females and 53 males; mean age, 56 years; age range, 32-79 years) were enrolled for analysis, and every patient had only one HCC lesion, including 59 cases that received specimen resection and 19 that received stereotactic biopsy. The tumors from these 78 subjects were classified as well differentiated (n=22), moderately differentiated (n=41) or poorly differentiated (n=15) HCC according to the criteria of Pathology and Genetics Tumors of the Digestive System (21). The clinicopathological characteristics of the patients are provided in Table I.

MRI protocol. Whole liver MRI scans were performed using a 3.0T system (Discovery™ MR750; GE Healthcare) with a 32-channel phased-array coil. Each patient was required to fast for 6-8 h prior to MRI. Conventional MRI, DWI, IVIM, DKI and contrast-enhanced MRI were performed together. The main imaging parameters are summarized below.

Axial 3D LAVA MRI (Discovery™ MR750; GE Healthcare) before and after contrast enhancement was performed using the following parameters: Repetition time/echo time (TR/TE), 3.6-4.4/1.7-1.9 msec; section thickness, 4.0 mm; intersection gap, 1 mm; matrix, 192x192; field of view (FOV), 32x32 cm; flip angle, 12˚; and number of excitations (NEX), 1. Axial fast-recovery fast spin-echo T2-weighted with fat suppressed images were obtained using the following parameters: TR/TE, 4,500-6,000/85-100 msec; section thickness, 4.0 mm; intersection gap, 1; matrix, 512x512; and FOV, 34x34 cm.

Conventional DWI was expressed by the following equation (7): S_b/S_0=exp (-b x ADC), where S_b and S_0 are the signal intensities in the diffusion gradient factors of b and 0, respectively. ADC could be calculated by fitting the signal with b-values of 0 and 800 sec/mm^2 to this model.

The IVIM model was expressed as follows (10): S_b/S_0=(1-f) exp (-b x D) + f exp [-b x (D + D^*)], where S_b and S_0 are the signal intensities in the diffusion gradient factors of b and 0, respectively. Three parameters, namely D, D^* and f, could be derived from IVIM by fitting the MRI signal acquired at 14 b-values (b=0, 5, 10, 15, 20, 25, 50, 80, 150, 300, 500, 600, 800 and 1,000 sec/mm^2), a section thickness of 3 mm, an intersection gap of 1 mm, a FOV of 320x320 mm and a NEX of 3 to a biexponential model. F is the perfusion fraction, while D is the diffusion coefficient representing pure molecular diffusion, and D^* is the pseudo-diffusion coefficient representing incoherent microcirculation within the voxel. For the IVIM model, a two-step fitting method was used to calculate the increase in robustness of the fitting with a lower calculation error, as follows: b >400 sec/mm^2 was fitted for the single parameter D, since D^* is significantly larger than D; thus, the influence of

Table I. Comparison of baseline characteristics between different pathological grades of HCC.

Baseline characteristics	Histological grading			P-value
	wHCC (n=22)	mHCC (n=41)	pHCC (n=15)	
Age, years	57.31±10.82	55.46±11.26	54.13±11.61	0.68
Sex (F/M)	8/14	13/28	4/11	0.82
Tumor size, cm	5.07±2.11	4.80±1.73	4.69±1.59	0.79

Continuous data are expressed as the mean ± standard deviation or n. HCC, hepatocellular carcinoma; w, well-differentiated; m, moderately differentiated; p, poorly differentiated; F, female; M, male.

pseudo-diffusion on signal decay could be neglected when the b-value was >400 sec/mm^2 (22).

The signal intensities of three b-values (b=0, 1,000 and 2,000 sec/mm^2) with 15 diffusion directions for every b-value, a section thickness of 4 mm, an intersection gap of 1 mm, a FOV of 320x320 mm, a NEX of 6 and an acquisition time of 8 min were used. DKI parameters, including MD and mean diffusional kurtosis (MK), were obtained with the following equation (11,12): $S_b/S_0=\exp[(-b \times D) + (b^2 \times D^2 \times K/6)]$, where S_b and S_0 are the signal intensities acquired with diffusion gradient factors of b and 0, respectively. D represents corrected ADC and K represents diffusion kurtosis. For the DKI model, empirical evidence indicates that maximum b-values of 2,000-3,000 sec/mm^2 are appropriate, and it is more efficient and convenient to simply use the b-values of 0, 1,000 and 2,000 sec/mm^2 (23,24).

For the axial 3D LAVA-Flex dynamic contrast-enhanced scan sequence (Discovery™ MR750; GE Healthcare), 20 ml gadolinium-diethylenetriaminepentaacetic acid (Magnevist; Schering AG) was rapidly administered intravenously at a speed of 2-3 ml/sec for a total dose of 0.2 mmol/kg of body weight using a double-tube high-pressure injector (MEDRAD® Spectris Solaris EP MR injection system; Bayer AG), alongside 20-ml sterile saline flush. For early, hepatic arterial, venous and delayed phases, the scans were set at 16, 30, 60 and 120 sec post-contrast injection, respectively.

Image analysis. The compiled data were computed using DKI, as well as mono and bi-exponential models. All original MR images were transferred to the workstation (Advantage Workstation v.4.4; GE Healthcare) for post-processing. To avoid selection bias to a greater extent, two radiologists with experience in hepatobiliary and gastrointestinal MRI for 12 and 8 years, respectively, performed the DKI, IVIM and DWI. Both were blinded to the results of the histopathological analysis. Regions of interest (ROIs) were manually traced on each slice of the DKI, IVIM and DWI (MK, MD, D, D*, f and ADC) to include the majority of the solid part of the tumor. Conventional pre- and post-contrast T2-weighted, contrast-enhanced and T1-weighted MR images were used for reference and to avoid regions of hemorrhage, cystic degeneration or necrotic areas. The mean ROI area was 67 mm^2 (range, 55-80 mm^2). The ROI was drawn multiple times (range, 2-4) on each lesion, depending on tumor size, and the mean value was calculated for analysis. The technique used is represented in Fig. 1.

Biopsy and histopathological examination. The tissue cylinders from the core biopsy were obtained by using an 18G cutting needle and biopsy gun (Magnum Bard). The penetration length ranged from 1.0 to 2.2 cm, which was selected according to the size and anatomical position of the lesion. The standard practice is to obtain 2-3 tissue cylinders. Subsequent specimens were obtained from various areas within the lesion by manually moving the outer needle to sample at random.

Tumor tissue specimens, which were obtained by post-surgical resection or stereotactic biopsy, were formalin-fixed (concentration, 10%; room temperature; duration, 6-48 h) and paraffin-embedded. The sections (thickness, 3 μm) were then stained with hematoxylin (room temperature; duration, 20 min) and eosin (room temperature; duration, 1 min) for pathological evaluation (Optical microscope, Leica DM2000 LED; Leica Microsystems; magnification, x200). A single pathologist, who had 15 years of experience in evaluating histopathological slices and was blinded to the findings of MRI, interpreted all the lesions. Each carcinoma was categorized cytologically as well-, moderately or poorly differentiated, according to the criteria of Pathology and Genetics Tumors of the Digestive System (20).

Statistical analysis. Statistical analysis was performed using SPSS v. 23.0 (IBM Corp.) and MedCalc v. 16.2.1 (MedCalc Software bvba) software. Data are expressed as the mean ± standard deviation (SD) of the three replicates. The data consistency of DKI-, IVIM- and DWI-derived parameters between both radiologists were evaluated by intraclass correlation coefficient (ICC) and Bland-Altman plot. ICC was indicative of good reliability when the measurements were >0.75, moderate reliability when the measurements were ≥0.4-<0.75, and poor reliability when they were <0.4. When the ICC was <0.75, repeat measurements of the corresponding DKI-, IVIM- and DWI-derived parameters were performed by the same reviewers (radiologists). Thereafter, the mean of 4 measurements was used as the final result for further analysis. The Mann-Whitney U-test and one-way ANOVA were used to compare differences in the DWI, IVIM and DKI parameters among different tumor grades. Spearman's correlation coefficient was performed to analyze the correlation between each parameter and pathological grade. In addition, Z test analysis was used to compare the receiver operating characteristic (ROC) curves of MK, MD, D, ADC, D* and f values to determine their performance in predicting highly differentiated

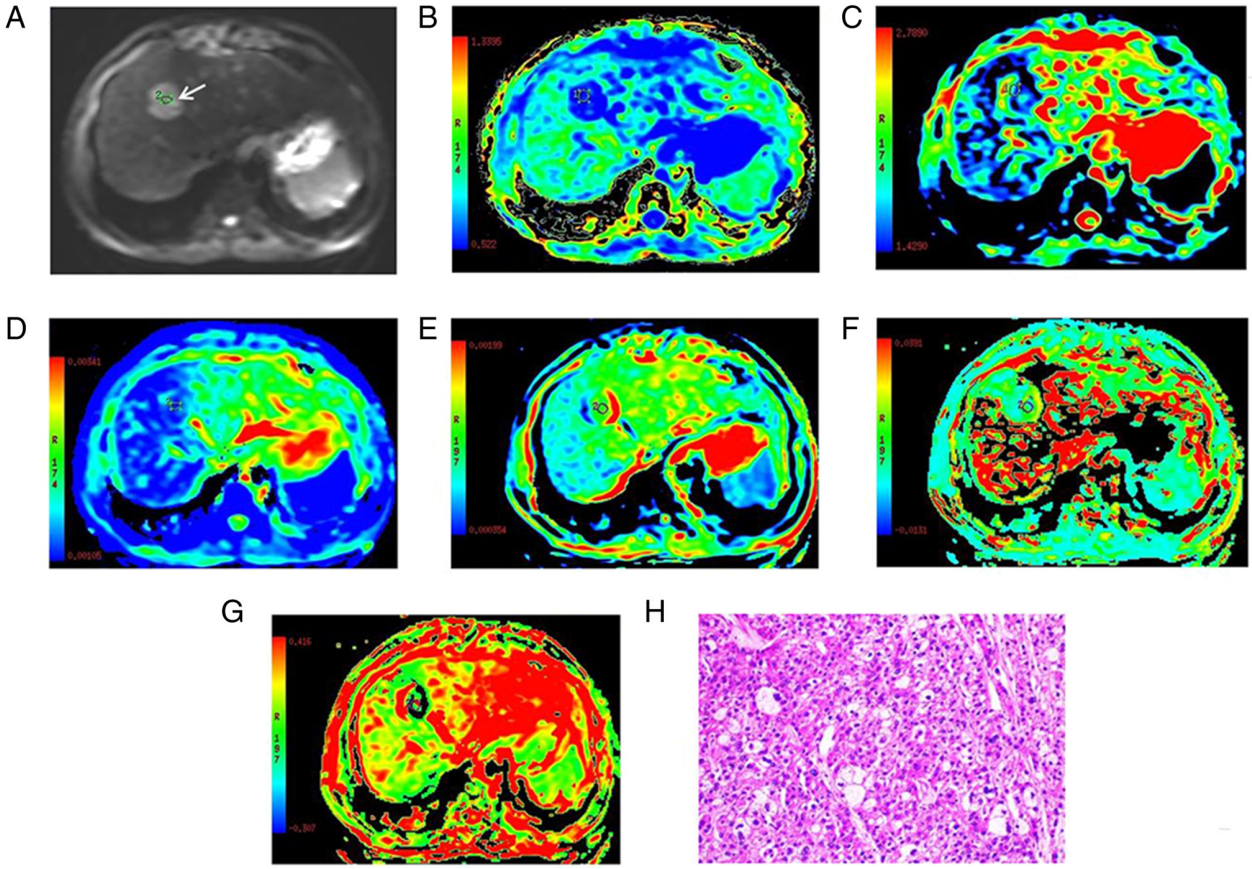

Figure 1. Images of a 52-year-old male with well-differentiated HCC at the anterior superior segment of the right lobe of liver, which are representative of all the patients with well-differentiated HCC enrolled in the present study. (A) DWI with a b-value of 800 sec/mm^2. (B-G) Parametric maps of (B) MK, (C) MD, (D) ADC, (E) D, (F) D* and (G) f calculated from the diffusion kurtosis imaging, intravoxel incoherent motion and DWI data. (H) Histologically, the HCC was confirmed as well differentiated by hematoxylin and eosin staining (magnification, x200). The tumor (white arrow in A) exhibited a high signal intensity on DWI. The MK, MD, ADC, D, D* and f values for the regions of interest of the HCC were 0.54, 1.71x10^{-3} mm^2/sec, 1.17x10^{-3} mm^2/sec, 1.09x10^{-3} mm^2/sec, 35.12x10^{-3} mm^2/sec and 0.19, respectively, which were indicative of well-differentiated HCC. HCC, hepatocellular carcinoma; DWI, diffusion-weighted imaging; MK, mean diffusional kurtosis; MD, mean diffusivity; ADC, apparent diffusion coefficient; D, true diffusion coefficient; D*, pseudo-diffusion coefficient; f, perfusion fraction.

HCC. The diagnostic accuracy, sensitivity and specificity were calculated with an optimal cutoff point determined by the point of the largest Youden index for each parameter. The tests were two-tailed, and P<0.05 was considered to indicate a statistically significant difference.

Results

Baseline characteristics and MRI appearance. The clinical and demographic characteristics of the 78 HCC patients (25 females and 53 males; mean age, 55.73±11.12 years; range, 32-79 years) are summarized in Table I. Out of these 78 subjects, 22 patients were pathologically diagnosed with well-differentiated HCC, 41 with moderately differentiated HCC and 15 with poorly differentiated HCC. The largest diameters of lesions ranged from 1.9 to 10.4 cm (mean, 4.9 cm). Fig. 1 shows MR diffusion images of a histopathologically confirmed case of well-differentiated HCC, which are representative of all patients with well-differentiated HCC enrolled in the present study.

Inter-observer reproducibility. The ICCs between the two radiologists for MK, MD, ADC, D, D*, f and ADC are shown in Table II. The results indicated that there was good reliability between the two observers for all parameters. Therefore, the mean measurement from the two observers was used as the final result in the current study.

Comparison between DKI-, IVIM- and DWI-derived parameters, and correlation analysis. The MK value of the well-differentiated HCC group was significantly lower than that of the moderately and poorly differentiated HCC groups (all P<0.01). The MD, D and ADC values of the well-differentiated HCC group were significantly higher than those of the moderately and poorly differentiated HCC groups (all P<0.05), whereas no significant difference was observed in D* or f (P=0.502 and 0.853, respectively). The quantitative comparison of the differences in the DKI-, IVIM- and DWI-derived parameters among the 3 groups are displayed in Fig. 2 and Table III.

The correlation coefficients among all the parameters and histopathological grades are shown in Table IV. Correlation analysis showed that the MK (r=0.705; P<0.001) values decreased from poor to moderately to well differentiated HCC, while the MD (r=0.570; P<0.001), ADC (r=0.423; P<0.001) and D (r=0.687; P<0.001) values were increased. MK was

Table II. Analysis of reliability between the two radiologists.

Diffusion parameter	ICC	95% CI	P-value
MK	0.927	0.889-0.953	<0.001
MD, $x10^{-3}$ mm^2/sec	0.910	0.863-0.942	<0.001
ADC, $x10^{-3}$ mm^2/sec	0.913	0.866-0.943	<0.001
D, $x10^{-3}$ mm^2/sec	0.953	0.928-0.970	<0.001
D^*, $x10^{-3}$ mm^2/sec	0.911	0.864-0.943	<0.001
f, %	0.851	0.776-0.903	<0.001

ICC, intraclass correlation coefficient; MK, mean diffusional kurtosis; MD, mean diffusivity; ADC, apparent diffusion coefficient; D, true diffusion coefficient; D^*, pseudo-diffusion coefficient; f, perfusion fraction.

negatively correlated with the degree of differentiation, while MD, D and ADC were positively correlated with it. However, the values of D* and f were not significantly correlated with the degree of differentiation.

Diagnostic performance of multiple parameters. The ROC curves of multiple parameters for evaluating highly differentiated HCC are shown in Fig. 3. The diagnostic accuracy, sensitivity and specificity of DKI-, IVIM- and DWI-derived parameters with the optimal cutoff point being determined by the point of the largest Youden index are shown in Table V. The comparison among the ROC curves of the MK, MD, D, ADC, D^* and f values for predicting highly differentiated HCC indicated that MK and D may be the best indicators for predicting highly differentiated HCC, as the AUC of the MK and D values were significantly higher than those of the ADC value (Z=2.247 and 2.428, P=0.025 and 0.016, respectively; Fig. 3), whereas no statistically significant differences in the AUC values of MK or D were observed (Z=0.072; P=0.942; Fig. 3). Furthermore, the combined diagnostic performance of the MK and D values exhibited higher accuracy, sensitivity and specificity, as the AUC of combined MK and D was significantly higher than that of each of these parameters alone (Z=2.044 and 2.106, P=0.041 and 0.035, respectively; Fig. 3).

Discussion

Despite being an invasive procedure, computed tomography/ultrasound-guided biopsy is also the main method of assessing the pathological grade of HCC. However, it has several limitations, such as requiring an appropriate site, the presence of complications and the risk of heterogenous tumors, which renders it challenging in routine clinical practice. It is therefore vital to establish preoperative tumor grading based on unbiased available data for the purpose of diagnosis (25). The ADC value derived from standard DWI has been found to be a valuable biomarker for predicting HCC grading, as it was reported to be inversely correlated with the pathological grade of HCC in previous studies (16-19). However, such ADC values were derived using a monoexponential Gaussian model, which is unsuitable for interpreting water diffusion (26). To the best of our knowledge, few studies in the literature have focused on comparing quantitative parameters derived from standard DWI, DKI and IVIM for detecting and grading HCC. The aim of the present study was to determine the diagnostic performance of parameters derived from DWI, IVIM and DKI for the assessment of the pathological grading of HCC.

The present study demonstrated that the application of ADC, D, MK and MD has both clinical practicability and value in differentiating HCC grades. The MD, D and ADC values were significantly higher in the well-differentiated HCC group than in the moderately and poorly differentiated HCC groups. As the tissues in these groups have a high cellular density and nuclear-to-cytoplasmic ratio, in addition to restricted extracellular space, the diffusion of water molecules is limited (27). Nishie *et al* (28) demonstrated that the ADC value was lower in poorly differentiated HCC than in well- and moderately differentiated HCC, which could contribute to the radiological diagnosis of poorly differentiated components in HCC. However, Nasu *et al* (20) found that the histopathological grade of 125 resected HCCs was not correlated with ADC, although higher-grade HCC displayed higher DWI and signal intensity. It was hypothesized that the pathological grading of tumors was mainly determined by the tumor's structural and cellular atypia, while the ADC mainly reflected structural atypia. Cellular atypia, expressed as the nucleus-to-cytoplasm ratio, is not fully represented by the current DWI model, as it is concerned with the extracellular Brownian motion rather than the intracellular water molecules. Therefore, evaluating pathological grade by ADC value alone could lead to incomplete results.

The results of the present study showed that the MK values in the well-differentiated HCC group were significantly lower than those in the moderately and poorly differentiated HCC groups, suggesting that MK values probably reflect the degree of tissue complexity. Well-differentiated HCC tends to have a lower cell density and abundant homogeneous nest of well-differentiated cells, while moderately and poorly differentiated HCCs have a higher degree of tissue complexity, microvascular invasion, and increased cellular density and nuclear-to-cytoplasmic ratio, including heterogeneity with necrosis and hemorrhage (21).

Furthermore, the present results demonstrated that the D^* and f values were not statistically significant in differentiating between well-, moderately and poorly differentiated HCC, which was in line with the findings of Zhu *et al* (29). This was mainly as HCC may have an abnormal perfusion area due to aberrant blood supply, and this feature may overlap in its histopathological grades. This may ultimately influence the D^* and f values, which are the perfusion parameters that reflect the vascularity of the tissue. Furthermore, previous studies have demonstrated that the D^* and f values have a large SD and poor reproducibility, which makes them prone to instability, thus decreasing their diagnostic potential (30,31). Nonetheless, Granata *et al* (32) demonstrated that the IVIM-derived f value could significantly differentiate high-grade HCC from low-grade HCC, and was positively correlated with the pathological grade of HCC, which was inconsistent with the present results; this reason may be related to differences in study subjects, MRI model and the selection of b values. Therefore, the association between the IVIM-derived f value and histological grade remains unclear.

Table III. Parameters derived from diffusion kurtosis imaging, intravoxel incoherent motion and diffusion-weighted imaging of different pathological grades of HCC.

	Histological grading				
Diffusion parameter	wHCC (n=22)	mHCC (n=41)	pHCC (n=15)	F-value	P-value
MK	0.62±0.06	0.73±0.05	0.78±0.06	43.10	<0.001
MD, x10^{-3} mm^2/sec	1.84±0.22	1.62±0.18	1.47±0.17	18.45	<0.001
ADC, x10^{-3} mm^2/sec	1.31±0.18	1.16±0.27	1.02±0.13	12.20	0.001
D, x10^{-3} mm^2/sec	1.24±0.11	0.99±0.12	0.92±0.10	43.64	<0.001
D^*, x10^{-3} mm^2/sec	32.20±11.11	29.56±8.39	29.05±9.76	0.70	0.502
f , %	22.89±6.21	21.99±6.09	22.25±5.69	0.16	0.853

Continuous data are expressed as the mean ± standard deviation. HCC, hepatocellular carcinoma; w, well-differentiated; m, moderately differentiated; p, poorly differentiated; MK, mean diffusional kurtosis; MD, mean diffusivity; ADC, apparent diffusion coefficient; D, true diffusion coefficient; D^*, pseudo-diffusion coefficient; f, perfusion fraction.

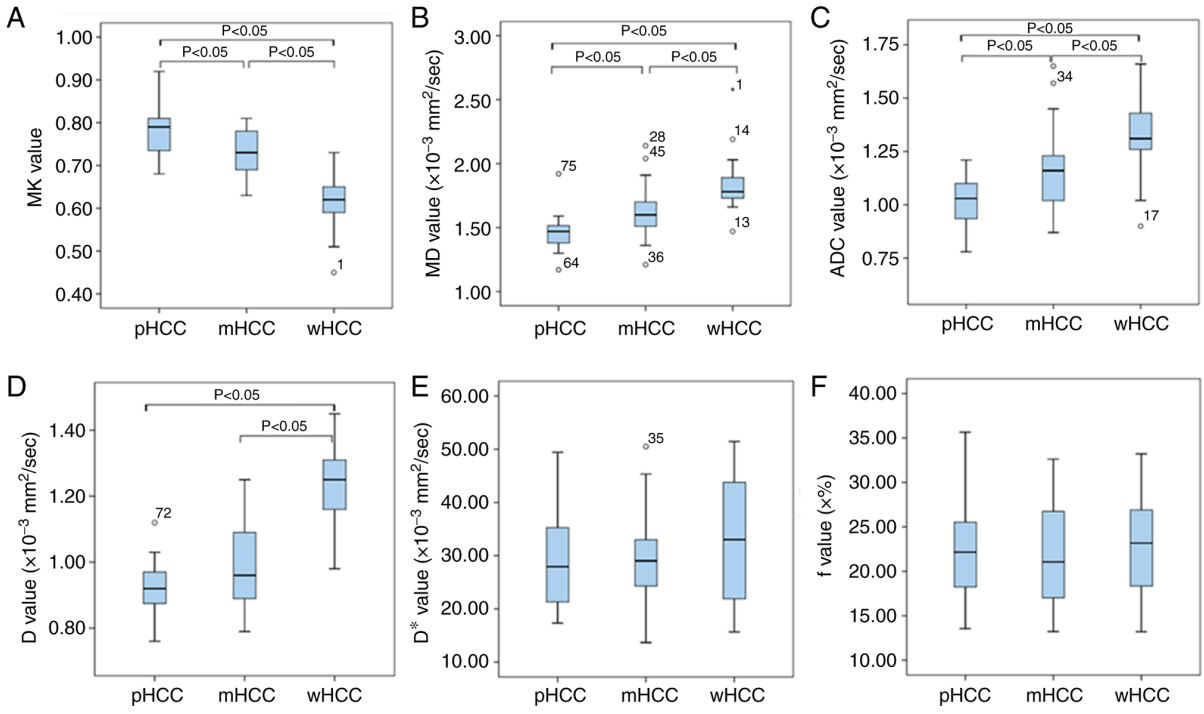

Figure 2. (A-F) Association between quantitative parameters and the histological grade of HCC. (A) MK, (B) MD, (C) ADC, (D) D, (E) D^* and (F) f values. HCC, hepatocellular carcinoma; w, well-differentiated; m, moderately differentiated; p, poorly differentiated; MK, mean diffusional kurtosis; MD, mean diffusivity; ADC, apparent diffusion coefficient; D, true diffusion coefficient; D^*, pseudo-diffusion coefficient; f, perfusion fraction.

Furthermore, these results demonstrated that the diagnostic performance of the MK and D values derived from DKI and IVIM, respectively, in differentiating well differentiated HCC from other types of HCC was higher than that of the DWI-derived ADC value. In addition, the combined diagnostic performance of MK and D values exhibited higher accuracy, sensitivity and specificity. Even though DWI reflected the characteristics of biological tissue through the movement of water molecules, the complex microstructures in biological tissues, including membranes, organelles and micro-capillary perfusion, can markedly influence water diffusion, for which the ADC value cannot accurately display the real diffusivity. Moreover, due to its intrinsic properties, the ADC value contains the combined information on both tissue cellularity (D) and perfusion (f) (33). Different grades of HCC, with their complex microstructure and presence of perfusion gradient, can affect the ADC values, resulting in signal loss, and thus decreased diagnostic performance during HCC evaluation. Therefore, the diagnostic value of ADC is controversial for detecting and grading HCC. The IVIM-derived D value is solely dependent on a molecular diffusion coefficient without any contributions from the microcirculation. Therefore, the diagnostic performance of D in differentiating well-differentiated HCC from other HCC types was higher than that of the ADC value. Furthermore, DKI was reported to quantify the non-Gaussian nature of water diffusion in biological tissues (11), which

Table IV. Spearman's correlation coefficients of the parameters derived from diffusion kurtosis imaging, intravoxel incoherent motion and diffusion-weighted imaging with histopathological grades.

	Histological grading				
Diffusion parameter	wHCC (n=22)	mHCC (n=41)	pHCC (n=15)	Correlation coefficient	P-value
MK	0.62±0.06	0.73±0.05	0.78±0.06	-0.705	<0.001
MD, x10^{-3} mm^2/sec	1.84±0.22	1.62±0.18	1.47±0.17	0.570	<0.001
ADC, x10^{-3} mm^2/sec	1.31±0.18	1.16±0.27	1.02±0.13	0.423	<0.001
D, x10^{-3} mm^2/sec	1.24±0.11	0.99±0.12	0.92±0.10	0.687	<0.001
D^*, x10^{-3} mm^2/sec	32.20±11.11	29.56±8.39	29.05±9.76	0.120	0.284
f, %	22.89±6.21	21.99±6.09	22.25±5.69	0.042	0.705

MK, mean diffusional kurtosis; MD, mean diffusivity; ADC, apparent diffusion coefficient; D, true diffusion coefficient; D^*, pseudo-diffusion coefficient; f, perfusion fraction.

Table V. Measurements of the threshold value, Youden index, sensitivity, specificity, accuracy and AUC of the MK, MD, ADC, D, D^* and f values for differentiating highly differentiated HCC from non-highly differentiated HCC.

Diffusion parameter	AUC (95% CI)	Optimal cutoff value	Youden index	Sensitivity (%)	Specificity (%)	Accuracy (%)
MK	0.946 (0.870-0.984)	0.69	0.75	90.9	83.9	85.90
MD, x10^{-3} mm^2/sec	0.844 (0.744-0.916)	1.65	0.69	95.5	73.2	79.49
ADC, x10^{-3} mm^2/sec	0.797 (0.691-0.880)	1.25	0.61	77.3	83.9	82.05
D, x10^{-3} mm^2/sec	0.943 (0.866-0.983)	1.10	0.71	90.9	80.4	83.33
D*, x10^{-3} mm^2/sec	0.573 (0.456-0.685)	34.11	0.25	50.0	75.0	67.95
f, %	0.541 (0.424-0.654)	23.89	0.18	50.0	67.9	62.82
Combined MK and D	0.994 (0.943-1.000)	0.13	0.95	100.0	94.6	96.15

HCC, hepatocellular carcinoma; MK, mean diffusional kurtosis; MD, mean diffusivity; ADC, apparent diffusion coefficient; D, true diffusion coefficient; D^*, pseudo-diffusion coefficient; f, perfusion fraction; AUC, area under the curve; CI, confidence interval.

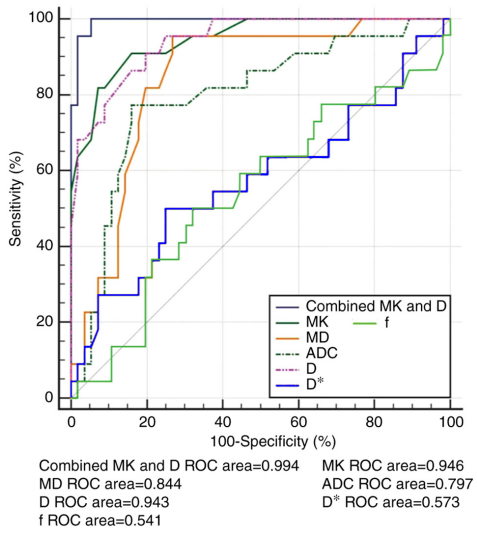

Figure 3. ROC curves of diffusion kurtosis imaging, intravoxel incoherent motion and diffusion-weighted imaging parameters of HCC to distinguish highly differentiated HCC from non-highly differentiated HCC. MK and D had the largest area under the curve of all the parameters. MK, mean diffusional kurtosis; MD, mean diffusivity; ADC, apparent diffusion coefficient; D, true diffusion coefficient; D^*, pseudo-diffusion coefficient; f, perfusion fraction; ROC, receiver operating characteristic.

suggests that it can more accurately reflect the diffusivity of water molecules in the tissue, while providing additional microstructural information about tissue heterogeneity and cellularity using high b-values (30).

The present study had several limitations. First, the sample size was relatively small and did not include cases of undifferentiated carcinoma. Further studies with a larger patient population are recommended. Secondly, 24.36% (19/78) of HCC cases were confirmed by histopathological analysis. However, the biopsy tissue may not be representative of the whole tumor, due to the cytopathological heterogeneity of tumors. Therefore, this sampling bias could have contributed to the disparity between each parameter and the cytopathological analysis. Furthermore, certain tumors were also present in the left lobe of the liver, and the ROIs in those tumors were prone to adjacent organ functions, such as gastrointestinal peristalsis, and heart and diaphragm motion. Finally, the present study did not evaluate the difference in prognosis between the histopathological grades of HCC based on the DKI, IVIM and ADC parameters, which should be a topic for further investigation.

In conclusion, the present study indicated that the MK and D values, derived from DKI and IVIM, respectively, are

feasible and helpful in distinguishing the histological grade of HCC and were superior to ADC. However, the conventional DWI using two b values with acceptable diagnostic efficiency and short scanning time remains a consideration for routine clinical application.

Acknowledgements

The authors would like to thank the English native speaker Professor Morgan A. McClure (Department of Radiology, Affiliated Hospital of North Sichuan Medical College, Nanchong, China) for helping to correct the grammar and structure of the manuscript.

Funding

No funding was received.

Availability of data and materials

The datasets generated and/or analyzed during the present study are available from the corresponding author on reasonable request.

Authors' contributions

HWL, YD, GWY and YJL contributed to the concept and design of the study; LHZ, HCY, XF, XXZ, RHF, JY, AB and HFY contributed to the literature search, data collection, statistical analysis and data interpretation; YD, JY and AB revised the manuscript. HWL, YD, YJL and GWY confirm the authenticity of all the raw data. All authors read and approved the final version of the manuscript.

Ethics approval and consent to participate

The present study was reviewed and approved by the Ethics Committee of the Affiliated Hospital of North Sichuan Medical College (Nanchong, China; approval no. nsmc17-10). Written informed consent was obtained from all the patients enrolled in the study.

Patient consent for publication

Not applicable.

Competing interests

The authors declare that they have no competing interests.

References

1. Bray F, Ferlay J, Soerjomataram I, Siegel RL, Torre LA and Jemal A: Global cancer statistics 2018: GLOBOCAN estimates of incidence and mortality worldwide for 36 cancers in 185 countries. CA Cancer J Clin 68: 394-424, 2018.
2. Izzo F, Palaia R, Albino V, Amore A, di Giacomo R, Piccirillo M, Leongito M, Nasto A, Granata V, Petrillo A and Lastoria S: Hepatocellular carcinoma and liver metastases: Clinical data on a new dual-lumen catheter kit for surgical sealant infusion to prevent perihepatic bleeding and dissemination of cancer cells following biopsy and loco-regional treatments. Infect Agent Cancer 10: 11, 2015.
3. Piccirillo M, Granata V, Albino V, Palaia R, Setola SV, Petrillo A, Tatangelo F, Botti G, Foggia M and Izzo F: Can hepatocellular carcinoma (HCC) produce unconventional metastases? Four cases of extrahepatic HCC. Tumori 99: e19-e23, 2013.
4. Poon RT, Fan ST, Lo CM, Liu CL and Wong J: Long-term survival and pattern of recurrence after resection of small hepatocellular carcinoma in patients with preserved liver function: Implications for a strategy of salvage transplantation. Ann Surg 235: 373-382, 2002.
5. Decaens T, Roudot-Thoraval F, Badran H, Wolf P, Durand F, Adam R, Boillot O, Vanlemmens C, Gugenheim J, Dharancy S, *et al*: Impact of tumor differentiation to select patients before liver transplantation for hepatocellular carcinoma. Liver Int 31: 792-801, 2011.
6. Zhou L, Rui JA, Wang SB, Chen SG, Qu Q, Chi TY, Wei X, Han K, Zhang N and Zhao HT: Factors predictive for long-term survival of male patients with hepatocellular carcinoma after curative resection. J Surg Oncol 95: 298-303, 2007.
7. Heijmen L, Ter Voert EE, Nagtegaal ID, Span P, Bussink J, Punt CJ, de Wilt JH, Sweep FC, Heerschap A and van Laarhoven HW: Diffusion-weighted MR imaging in liver metastases of colorectal cancer: Reproducibility and biological validation. Eur Radiol 23: 748-756, 2013.
8. Kele PG and van der Jagt EJ: Diffusion weighted imaging in the liver. World J Gastroenterol 16: 1567-1576, 2010.
9. Wan Q, Deng YS, Zhou JX, Yu YD, Bao YY, Lei Q, Chen HJ, Peng YH, Mei YJ, Zeng QS and Li XC: Intravoxel incoherent motion diffusion-weighted MR imaging in assessing and characterizing solitary pulmonary lesions. Sci Rep 7: 43257, 2017.
10. Yuan J, Yeung DK, Mok GS, Bhatia KS, Wang YX, Ahuja AT and King AD: Non-Gaussian analysis of diffusion weighted imaging in head and neck at 3T: A pilot study in patients with nasopharyngeal carcinoma. PLoS One 9: e87024, 2014.
11. Le Bihan D, Breton E, Lallemand D, Grenier P, Cabanis E and Laval-Jeantet M: MR imaging of intravoxel incoherent motions: Application to diffusion and perfusion in neurologic disorders. Radiology 161: 401-407, 1986.
12. Jensen JH and Helpern JA: MRI quantification of non-Gaussian water diffusion by kurtosis analysis. NMR Biomed 23: 698-710, 2010.
13. Jensen JH, Helpern JA, Ramani A, Lu H and Kaczynski K: Diffusional kurtosis imaging: the quantification of non-gaussian water diffusion by means of magnetic resonance imaging. Magn Reson Med 53: 1432-1440, 2005.
14. Weber RA, Hui ES, Jensen JH, Nie X, Falangola MF, Helpern JA and Adkins DL: Diffusional kurtosis and diffusion tensor imaging reveal different time-sensitive stroke-induced microstructural changes. Stroke 46: 545-550, 2015.
15. Zhu J, Zhuo C, Qin W, Wang D, Ma X, Zhou Y and Yu C: Performances of diffusion kurtosis imaging and diffusion tensor imaging in detecting white matter abnormality in schizophrenia. Neuroimage Clin 7: 170-176, 2014.
16. Guo W, Zhao S, Yang Y and Shao G: Histological grade of hepatocellular carcinoma predicted by quantitative diffusion-weighted imaging. Int J Clin Exp Med 8: 4164-4169, 2015.
17. Chen J, Wu M, Liu R, Li S, Gao R and Song B: Preoperative evaluation of the histological grade of hepatocellular carcinoma with diffusion-weighted imaging: A meta-analysis. PLoS One 10: e0117661, 2015.
18. Li X, Li C, Wang R, Ren J, Yang J and Zhang Y: Combined application of gadoxetic acid disodium-enhanced magnetic resonance imaging (MRI) and diffusion-weighted imaging (DWI) in the diagnosis of chronic liver disease-induced hepatocellular carcinoma: A meta-analysis. PLoS One 10: e0144247, 2015.
19. Woo S, Lee JM, Yoon JH, Joo I, Han JK and Choi BI: Intravoxel incoherent motion diffusion-weighted MR imaging of hepatocellular carcinoma: Correlation with enhancement degree and histologic grade. Radiology 270: 758-767, 2014.
20. Nasu K, Kuroki Y, Tsukamoto T, Nakajima H, Mori K and Minami M: Diffusion-weighted imaging of surgically resected hepatocellular carcinoma: Imaging characteristics and relationship among signal intensity, apparent diffusion coefficient, and histopathologic grade. AJR Am J Roentgenol 193: 438-444, 2009.
21. Stanley R. Hamiton and Lauri A: altonen. Pathology & genetics tumors of the digestive system (the Master Translator: Yu JY, Cu QC)[M]. BeiJing, People's Medical Publishing House 202, 2006.
22. Le Bihan D, Turner R and MacFall JR: Effects of intravoxel incoherent motions (IVIM) in steady-state free precession (SSFP) imaging: Application to molecular diffusion imaging. J Magn Reson Med 10: 324-337, 1989.

23. Glenn GR, Helpern JA, Tabesh A and Jensen JH: Quantitative assessment of diffusional kurtosis anisotropy. NMR Biomed 28: 448-459, 2015.
24. Lätt J, Nilsson M, Malmborg C, Rosquist H, Wirestam R, Ståhlberg F, Topgaard D and Brockstedt S: Accuracy of q-space related parameters in MRI: Simulations and phantom measurements. IEEE Trans Med Imaging 26: 1437-1447, 2007.
25. Stigliano R, Marelli L, Yu D, Davies N, Patch D and Burroughs AK: Seeding following percutaneous diagnostic and therapeutic approaches for hepatocellular carcinoma. What is the risk and the outcome? Seeding risk for percutaneous approach of HCC. Cancer Treat Rev 33: 437-447, 2007.
26. Iima M and Le Bihan D: Clinical intravoxel incoherent motion and diffusion MR imaging: Past, present, and future. Radiology 278: 13-32, 2016.
27. Le Moigne F, Boussel L, Haquin A, Bancel B, Ducerf C, Berthezène Y and Rode A: Grading of small hepatocellular carcinomas (≤2 cm): Correlation between histology, T2 and diffusion-weighted imaging. Br J Radiol 87: 20130763, 2014.
28. Nishie A, Tajima T, Asayama Y, Ishigami K, Kakihara D, Nakayama T, Takayama Y, Okamoto D, Fujita N, Taketomi A, *et al*: Diagnostic performance of apparent diffusion coefficient for predicting histological grade of hepatocellular carcinoma. Eur J Radiol 80: e29-e33, 2011.
29. Zhu SC, Liu YH, Wei Y, Li LL, Dou SW, Sun TY and Shi DP: Intravoxel incoherent motion diffusion-weighted magnetic resonance imaging for predicting histological grade of hepatocellular carcinoma: Comparison with conventional diffusion-weighted imaging. World J Gastroenterol 24: 929-940, 2018.
30. Luo M, Zhang L, Jiang XH and Zhang WD: Intravoxel Incoherent Motion Diffusion-weighted Imaging: Evaluation of the differentiation of solid hepatic lesions. Transl Oncol 10: 831-838, 2017.
31. Sun H, Xu Y, Xu Q, Shi K and Wang W: Rectal cancer: Short-term reproducibility of intravoxel incoherent motion parameters in 3.0T magnetic resonance imaging. Medicine (Baltimore) 96: e6866, 2017.
32. Granata V, Fusco R, Catalano O, Guarino B, Granata F, Tatangelo F, Avallone A, Piccirillo M, Palaia R, Izzo F and Petrillo A: Intravoxel incoherent motion (IVIM) in diffusion-weighted imaging (DWI) for Hepatocellular carcinoma: Correlation with histologic grade. Oncotarget 7: 79357-79364, 2016.
33. Chandarana H, Lee VS, Hecht E, Taouli B and Sigmund EE: Comparison of biexponential and monoexponential model of diffusion weighted imaging in evaluation of renal lesions: Preliminary experience. Invest Radiol 46: 285-291, 2011.